First-principles determination of the effect of boron on aluminum grain boundary cohesion

Shengjun Zhang,[1,2,*] Oleg Y. Kontsevoi,[2] Arthur J. Freeman,[1,2] and Gregory B. Olson[1]
[1]*Department of Materials Science and Engineering, Northwestern University, Evanston, IL 60208, USA*
[2]*Department of Physics and Astronomy, Northwestern University, Evanston, IL 60208, USA*
(Received 6 July 2011; revised manuscript received 22 September 2011; published 17 October 2011)

Despite boron being a common alloying element in aluminum, its segregation into the aluminum grain boundary and its effect on the grain boundary strength have not been studied. Here, the electronic structures of the boron-doped $\Sigma5(012)[100]$ symmetrical tilt grain boundary and (012) free surface systems for aluminum are investigated by means of first-principles calculations using the full-potential linearized augmented plane-wave method with the generalized gradient approximation, within the framework of the Rice-Wang thermodynamic model and the theoretical tensile test approach. We establish that boron has a large driving force to segregate from Al bulk to the symmetrical grain boundary hollow site, and its segregation significantly enhances the grain boundary strength. Through precise calculations on both the grain boundary and free surface environments, it is found that boron is a strong cohesion enhancer in aluminum with a potency of -0.19 eV/atom. An analysis in terms of the relaxed atomic and electronic structures and bonding characters shows that the aluminum-boron bond has mixed covalent and metallic character and is strong in both grain boundary and free surface environments. The strengthening effect of boron is due to creation of additional B–Al bonds across the grain boundary, which are as strong as existing Al–Al transgranular bonds and thus significantly increase grain boundary adhesion and its resistance to tensile stress and cracking.

DOI: 10.1103/PhysRevB.84.134104 PACS number(s): 61.72.Mm, 62.20.mm, 68.35.Dv, 31.15.A−

I. INTRODUCTION

Rising fuel prices and increasing demands for fuel economy in transportation vehicles lead to considerable efforts to understand and enhance the structural properties in aluminum alloys due to their attractive lightweight characteristics. Boron (B) is widely used as a grain refiner in aluminum alloys to improve their strength, especially by precipitating vanadium, titanium, chromium, and molybdenum.[1] Although B has a good record in improving the intergranular cohesion in metals, especially in Fe and Ni,[2] its effect on the grain boundary (GB) cohesion in Al is largely unknown, and no systematic experimental or theoretical studies have been reported in the open literature. According to the Al-B phase diagram, the solid solubility of B in Al is negligible, which indicates that the dissolved B in Al may have a strong propensity to segregate to interfaces and surfaces. However, it is not clear how high its segregation energy is or whether the segregation weakens or strengthens Al GBs.

Boron has been shown via first-principles investigations to be a good GB cohesion enhancer in a number of transition metals, including Fe,[3] Ni,[4,5] Mo,[6] and Cu,[7] while the behavior of B in Al GBs is still unknown. In this work, a comprehensive study is performed to investigate the effect of B in the Al GB using both the Rice-Wang model[8] and the *ab initio* computational tensile test. The highly precise full-potential linearized augmented plane-wave (FLAPW) method is employed.[9] At first, the segregation energy of B from Al bulk to the Al GB is calculated to validate the driving force of B segregation. Then, the electronic properties of fully relaxed atomic structures of B/Al $\Sigma5(012)[100]$ GB and the corresponding B/Al (012) free surface (FS) are obtained by minimizing the total energies as directed by the calculated atomic forces. Following that, the GB fracture energy is calculated to determine the favored GB facture mode energetically. The Rice-Wang model is used to obtain the B effect on Al GB cohesion quantitatively. The *ab initio* computational tensile test procedure allows a close examination of the process of the GB breaking at an electronic level. Finally, the calculated atomic and electronic features and theoretical tensile test data are used to analyze the physics that dominate the embrittling or strengthening behavior of B in the Al GB.

II. MODEL AND COMPUTATION

The Al $\Sigma5(012)[100]$ tilt GB was chosen as a representative GB because, according to experiments,[10] it is one of the high-energy and stable GBs in Al (for more detail on the GB selection, see Ref. 11). The initial crystal structure of the GB is based on the coincident site lattice (CSL) model; the results of selection, optimization, and validation of the Al GB model were presented in our previous work.[12] The crystal structure of the Al $\Sigma5(012)[100]$ GB used in this work is shown in Fig. 1(a); it consists of 25 layers marked 1 to 13 and -2 to -13. The B atoms, due to their small size, occupy interstitial positions in Al; in the GB, one B atom will occupy the GB hollow site, which is marked as "Site 0" in Fig. 1. The FS models represent the GB after it fractures. For the Al (012) FS, the Al (012) substrate plane is simulated by a 13-layer slab and a 12-layer slab. The 13-layer slab FS contains the core atom (site 1) from the GB, while the 12-layer slab FS does not. The other side of FS (sites –11/11, –12/12, and –13/13) is treated as a bulk-like structure.

The electronic structure was calculated using the full-potential linearized augmented plane-wave (FLAPW) method for thin films,[9] which has been proven to be one of the most accurate methods for the computation of the electronic structure of surfaces and solids within density functional theory. No shape approximations were made to the charge densities, potentials, and matrix elements. For both the Al and B atoms, the core states were treated fully relativistically, and the valence states were treated semirelativistically (i.e., without

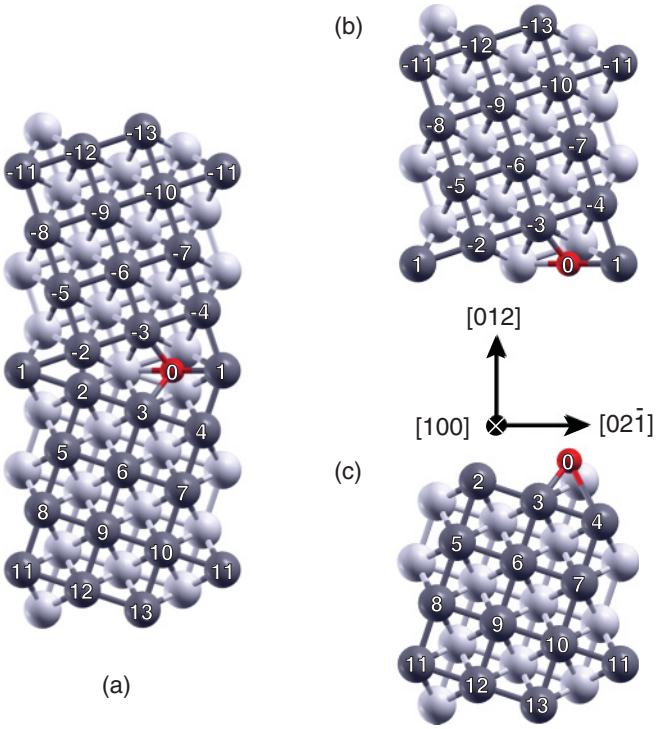

FIG. 1. (Color online) Crystal structures of the computational cell of the GB and FS: (a) an Al $\Sigma5(012)[100]$ GB with an interstitial atom in the GB hollow site marked 0; (b) a 13-layer Al (012) FS with an interstitial atom; and (c) a 12-layer Al (012) FS with an interstitial atom. The atomic sites are labeled by numbers counted from the GB plane. The structures repeat along the [02$\bar{1}$] direction. The dark-gray and light-gray atoms represent atoms in layers with $y = 0$ (in the paper plane) and $y = 0.5$ (beneath the paper plane) along the [100] direction, respectively. Site 1 is on the mirror plane, which is also the GB plane; site 0 is the GB hollow site; sites i and $-i$ ($i = 2$ to 13) have mirror symmetry. The three directions [100], [012], and [02$\bar{1}$]are shown by arrows. The [012] direction is parallel to the z axis, the length of which is optimized for the GB case.

spin-orbit coupling). The exchange-correlation contribution to the potential was included using the generalized gradient approximation (GGA) within the Perdew-Burke-Ernzerhof functional.[13] An energy cutoff of 218 eV was employed for the augmented plane-wave basis to describe the wave functions in the interstitial region, and an 1100 eV cutoff was used for the star functions depicting the charge density and potential. Muffin-tin radii were chosen to be 2.3 atomic units (a.u.) and 1.3 a.u. for Al and B, respectively, and a two-dimensional (2D) **k**-point mesh of 7×7 was employed. Within the muffin-tin spheres, lattice harmonics with angular momentum quantum number l up to 8 were adopted.

Convergence was assumed when the average root-mean-square differences between the input and output charge and spin densities were less than $1\times10^{-5}e/(\text{a.u.})^3$. To simulate the bulk-like environment for the GB and FS cases, the positions of the three outermost Al layers (sites 11, 12, 13, and -11, -12, -13) were fixed to their face-centered cubic (fcc) coordination and distances as in bulk Al; all other atoms in the unit cells were fully relaxed by force minimization. Equilibrium relaxed structures were assumed when the atomic forces on each atom became less than 0.01 eV/a.u..

III. SEGREGATION ENERGY OF BORON

As a first step in calculations of the impurity effect on the GB, one must ascertain that there is in fact a driving force for the impurity atom to segregate at the GB. Since the size of the B atom is much smaller than that of the Al atom (covalent radii of Al and B are 0.121 nm and 0.084 nm, respectively)[14], it is assumed to occupy interstitial positions in both bulk Al and the GB. The octahedral interstitial O_h, the largest interstitial in the fcc structure, surrounded by Al atoms in sites 5, 6, 8, and 9 and away from both the GB plane and the surface of the cell, was chosen to represent a B atom segregated in Al bulk, and the hollow site 0 is the segregation site for B in the GB.

In order to find equilibrium geometries of the GB with a B atom in the interstitial and GB hollow sites, series of total energy calculations were carried out in which the unit cell sizes were increased in the direction normal to the GB plane in small increments, starting from the CSL model size. For each increment, the total energy of the system was calculated with full relaxation. The minimum of the curve of the total energy of the GB system vs the expansion corresponds to the equilibrium GB state.

The total energies of the system vs the expansion distance are plotted in Fig. 2. The GB with a B atom in the octahedral interstices is expanded by 0.85 a.u. compared to the expansion of the pure Al GB of 0.45 a.u.[12] On the other hand, the B atom in the GB hollow site does not expand the GB: The expansion distance is the same (0.45 a.u.) as for the pure Al GB. This indicates that the GB hollow site is large enough to accommodate one B atom without causing any additional distortions to the GB, and that there could be a strong driving force for the B atom to move from a bulk interstitial to a GB hollow site, which would significantly reduce the mechanical energy of the system.

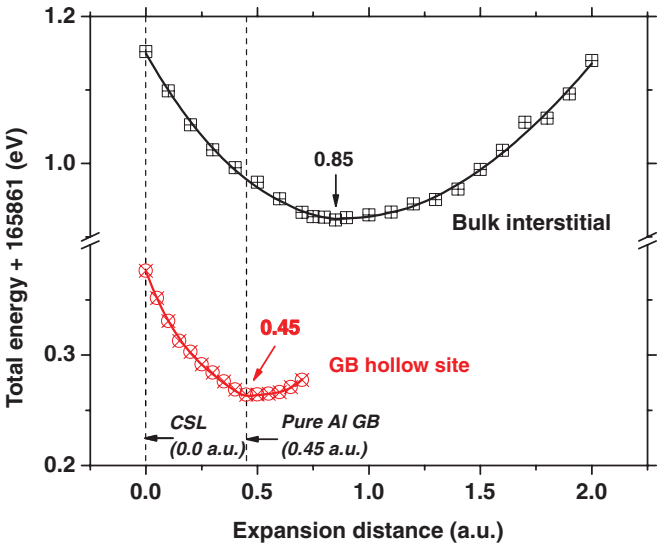

FIG. 2. (Color online) Total energies of the GB with a B atom in the bulk interstitial site and in the GB hollow site with respect to expansion distances of the cell relative to CSL model size.

TABLE I. Calculated segregation energies, binding energies, and embrittling potencies of a B atom in the Al GB.

Position	Expansion distance (a.u.)	Segregation energy (eV/atom)	Fracture path Mode	Part I	Part II	Fracture energy (J/m^2)	Embrittling potency (eV/atom)	Effect on GB
Site 0	0.45	−0.66	I	12-layer Al	13-layer + B	2.03	−0.56	Cohesion enhancer
			II	13-layer Al	12-layer + B	1.70	−0.19	Cohesion enhancer

This driving force is the segregation energy, which can be calculated as the difference in the total energy of the system with the B atom in the GB hollow site and the total energy of the GB system with the B atom in the bulk interstitial site. As listed in Table I, the calculated segregation energy of B from Al octahedral interstitial to the Al GB hollow site is −0.66 eV/atom, which indicates a high driving force favoring GB segregation. Note that because of the limited size of the 2D-periodic GB cell, the B atoms in the bulk interstitials are not well distributed randomly, and the concentration of B in the supercell is not dilute ($C_B = 3.85$ at.%). Therefore, the segregation energy calculated here may not accurately reflect B in the dilute limit in Al bulk and should be considered only as an estimate. Nevertheless, according to the magnitude of the segregation energy and considering the negligible solid solubility of B in bulk Al, one expects GBs to be saturated with B.

IV. FRACTURE ENERGY AND FRACTURE PATH OF GB

The measure of the GB strength is its fracture energy, ΔE_{frac}, which is defined as the difference between the total energy of an unbroken GB, E_{GB}, and the total energies of the resulting two free surfaces, E_{FS1} and E_{FS2}, per unit cell area S of the cleavage plane: $\Delta E_{\text{frac}} = (E_{\text{GB}} - E_{\text{FS1}} - E_{\text{FS2}})/\text{S}$. There could be several possible ways ("fracture paths") that the GB can break, and the corresponding fracture energies should be compared to determine the preferred fracture path. From the crystal structure in Fig. 1(a), one can see that the bonds along the GB mainly include the bonds between atoms 1 and 2(−2), 1 and 4(−4), 0 and 3(−3), 2 and −2, and 0 and 1. Assuming that the mirror symmetry remains after B segregates to the site 0 (which will be confirmed later), there are two facture paths that follow the Al GB as shown schematically in Fig. 3. In path I, the core Al(1) atom remains on the same grain with the segregated B atom after the fracture; in path II, the core Al(1) atom and the B atom stay on the different grains. For the pure GB, fracture paths I and II are identical due to mirror symmetry, and their fracture energy is the same, as reported in our previous work.[12]

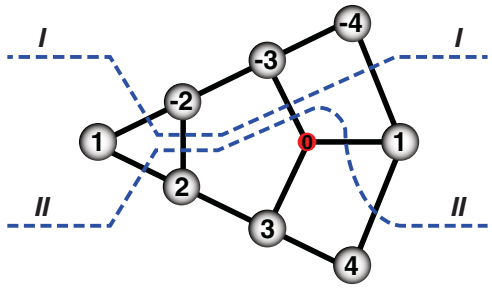

FIG. 3. (Color online) Schematic diagrams of the fracture paths for the Al GB with a B atom in site 0. Fracture surfaces are marked with dashed lines.

The calculated fracture energies of the two paths are listed in Table I. Fracture path II has a lower fracture energy, which indicates that the B is favored energetically to stay on the 12-layer FS after the GB breaks. [The crystal structure of the 12-layer FS with a B atom is shown in Fig. 1(c).] From these calculations, it can be concluded that the GB will follow fracture path II during breakup, as it will result in the lowest-energy state.

V. EMBRITTLEMENT POTENCY OF B WITHIN THE RICE-WANG THERMODYNAMIC MODEL

The embrittlement potency concept is based on a thermodynamic theory developed by Rice and Wang,[8] which describes the mechanism of intergranular embrittlement through the competition between plastic crack blunting and brittle boundary separation. The potency of a segregation impurity in reducing the "Griffith work"[15] of brittle boundary separation is a linear function of the difference in binding energies for that impurity at the GB and at the FS.

According to the Rice-Wang model, the embrittling potency is defined as

$$\Delta E = \left(E^B_{\text{GB}} - E_{\text{GB}}\right) - \left(E^B_{\text{FS}} - E_{\text{FS}}\right), \tag{1}$$

where E_{GB}, E^B_{GB},E_{FS}, and E^B_{FS} represent the total energies of the clean GB, B-segregated GB, clean FS, and B-adsorbed FS slabs, respectively. Values for $E_{\text{GB}}$and E_{FS} were taken from our previous work.[12] The calculated ΔE values are presented in Table I. The embrittlement potency is −0.56 eV/atom in fracture path I and −0.19 eV/atom in fracture path II, and the difference is due to dissimilar local atomic configurations of B on the different FSs. Quantitatively, it can be interpreted as the difference in the adsorption energy between B adatoms in different positions on the Al (012) surface, as shown in Figs. 1(b) and 1(c). As can be seen here and as was demonstrated in our previous works,[11,12] the choice of a fracture path has a significant impact on the calculated embrittling or strengthening effect of impurities in the GB, and an incorrect choice of the fracture path may result in a qualitatively incorrect prediction of the embrittling or strengthening behavior of the impurity. In the case of B, the embrittling potencies of B have a negative sign in both fracture paths, meaning that B is a cohesion enhancer in the Al GB in both cases. Of these two, only fracture path II, which has lower

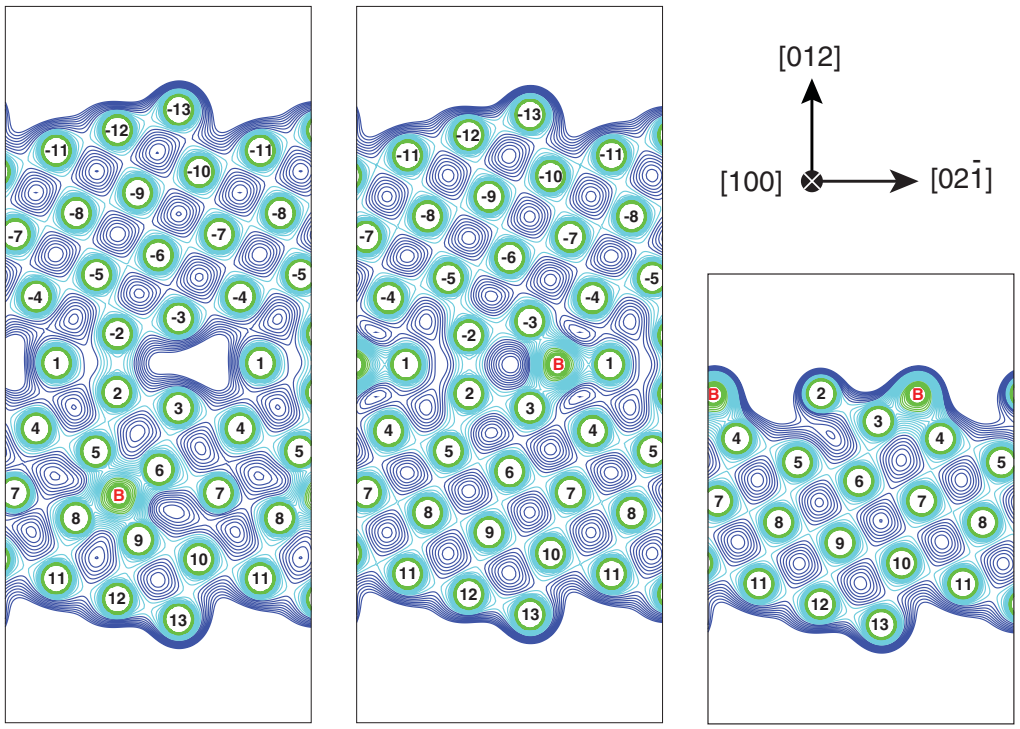

FIG. 4. (Color online) The calculated charge densities for (a) the Al GB with a B atom in the bulk interstitial site, (b) the Al GB with a B atom in the GB hollow site, and (c) the 12-layer Al FS with a B atom. Contours start from 0.01 $e/(\text{a.u.})^3$ and increase successively by a factor of $2^{1/8}$.

fracture energy, is the true path, and therefore the embrittling potency of B in the Al GB is −0.19 eV/atom.

VI. ELECTRONIC STRUCTURE AND BONDING CHARACTER

The effect of B on the interatomic bonding characteristics of the Al GB was investigated on the basis of calculated charge densities, electronic densities of states (DOS), and bond lengths. Figure 4 shows contour plots of the charge density distribution for valence electrons in the (100) plane for the Al GB with a B atom in the bulk interstitial site, the Al GB with a B atom in the GB hollow site, and the 12-layer Al FS with a B atom. The calculated local density of states (LDOS) for the Al GB with B in site 0 and the LDOS for the 12-layer Al FS with B are presented in Fig. 5. It can be seen from Fig. 4(a) that the B atom inserted in the Al bulk interstitial site does not affect the charge density distribution near the GB, as well as near both end-sides of the cell, which indicates that the site is a good bulk site to put an interstitial atom. The B atom forms bonds with the neighbor Al atoms—Al(5), Al(6), Al(8), and Al(9)—and expands the structure along the z axis, which is shown by the charge density reduction between Al atoms (e.g., Al(4)–Al(7) and Al(7)–Al(10)). The expansion agrees with the results of Fig. 2.

The introduction of a B atom in the GB hollow site causes the charge density to increase significantly in the GB region, and new directional B–Al bonds are formed, B–Al(1), B–Al(3), and B–Al(−3), as seen in Fig. 4(b). According to Fig. 2, B segregation does not lead to structure expansion; the GB hollow site appears to have a perfect size to accommodate one B atom, and its segregation there does not lead to significant relaxation of neighboring Al atoms, as judged from the interatomic distances in Fig. 6. Figure 5 (Part I) shows the s- and p-electron contributions to the local LDOS for the B atom in site 0 and Al atoms in sites 1, 2, and 3 and the B atom in site 0, respectively. Excepting the spurious small peaks originating from the Al surface and GB states, the p-electron LDOS values for B and all Al atoms are very similar and have near-free-electron shape. This indicates that the p-states of Al and B are delocalized and participate in metallic bonding. The s-states of B are more localized, forming a packet of states between −12 and −8 eV. These states hybridize with s-states of Al atoms in sites 1, 2, and 3, which also form packets of electron density between −12 and −8 eV. This hybridization is indicative of a covalent type of bonding. Thus, the B-Al bonding has mixed metallic-covalent character, with the metallic contribution dominating. We should note that B and Al are electronic analogs: They both have 3 valence electrons in an s^2p^1 configuration, and from this analogy, one could expect similar, metallic character of B-Al bonding. On the other hand, B is a much smaller atom, and there is a notable difference between electronegativities of these elements (1.61 Pauling units for Al and 2.04 for B), which would favor more directional bonding. Therefore, from the electronic point of view, one can expect a competition between metallic and covalent bonding, and the outcome of this competition ultimately depends on the local atomic configuration. To gain

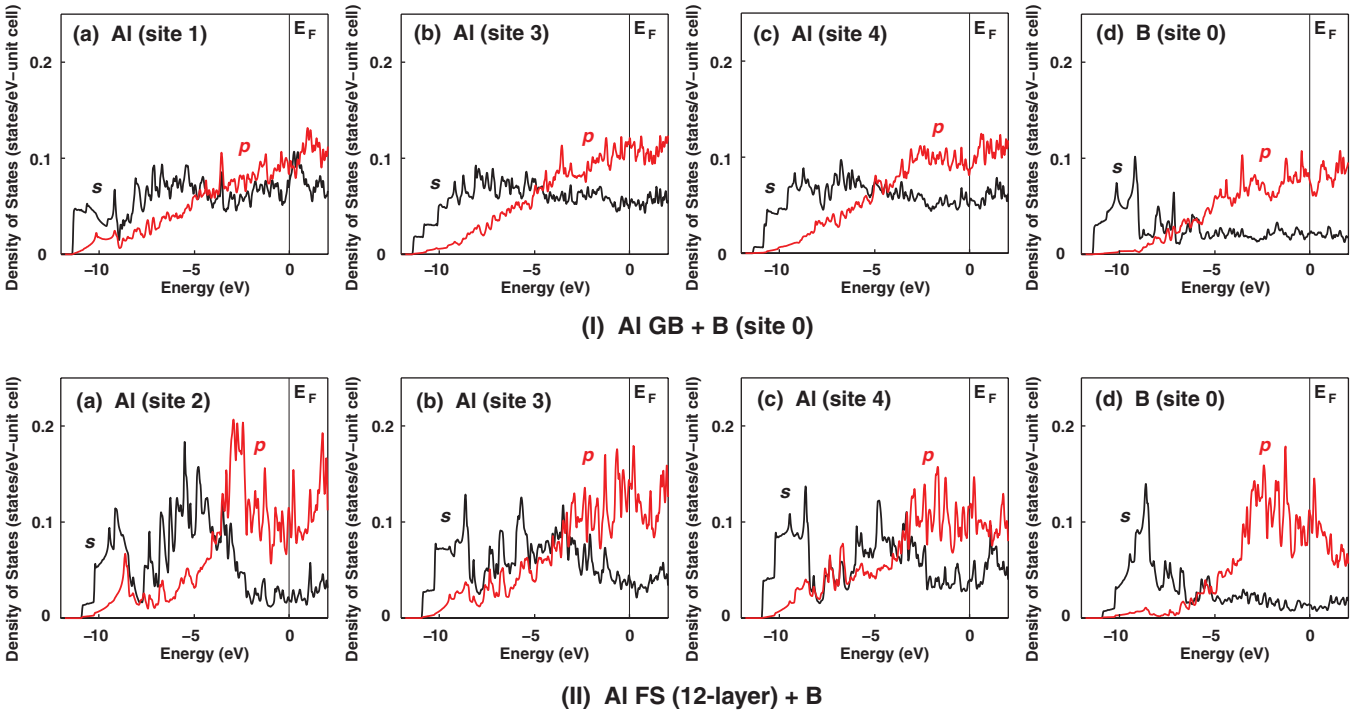

FIG. 5. (Color online) Calculated density of states with respect to the energy for (I) the Al GB with B in site 0 and (II) the Al FS with B. The Fermi energy is indicated by E_F.

more insight into the bonding character, we will consider the local atomic coordination of a B atom segregated in the Al GB, which is shown in Fig. 6(a). There, the B atom has 7 nearest-neighbor Al atoms and forms bonds with all of them. Segregated B does not expand or contract the GB, which means that the B–Al bonds are at near-ideal length. Despite the very peculiar 7-fold coordination, the strength of these bonds is almost equal, as judged by the very close bond lengths and equal charge density distribution between those bonds. Since most electrons of Al atoms in sites 1, 2, and 3 are delocalized, there are not enough of them left to form fully directional covalent bonding with B. Therefore, for B segregated in the Al GB, its bonding character with Al is mixed—metallic with B*s*Al*s* covalent contribution.

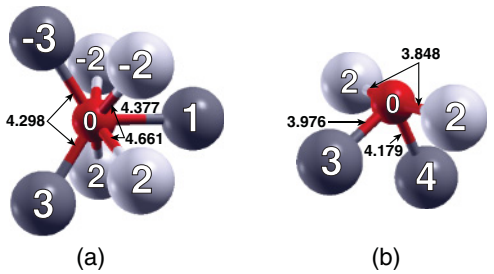

FIG. 6. (Color online) Nearest-neighbor configuration of the segregated B atom (shown in red) in (a) the Al GB, and (b) the Al FS, and the length of B–Al bonds (in a.u.). Similar to Fig. 1, the dark-gray spheres represent Al atoms in layers with $y = 0$ (in the paper plane), and light-gray spheres illustrate Al atoms with $y = 0.5$ and $y = -0.5$ (beneath and above the paper plane) along the [100] direction.

The situation is notably different for B at the Al surface, which forms after the GB has broken. Figure 4(c) shows the calculated charge density of the fractured surface in the (100) plane passing through the B atom, and Fig. 6(b) presents the local nearest-neighbor coordination of the B atom. One can see that the B atom now has only four bonds with nearest-neighbor Al atoms, Al(3), Al(4), Al(2), and Al(−2), and these bonds are stronger than the B–Al bonds in the GB, as judged from the higher bonding charge density and shorter bond length (cf. Fig. 6). On the FS, each of the Al(2) atoms is connected with two B atoms to form a strong bonding with the shortest bond lengths (3.848 a.u.). As a result of this, the bonding of the Al(2) atom with the rest of the Al surface is weakened, as is clearly seen from the charge density plot in Fig. 4(c): The Al(2) –Al(5) bonding almost disappears, and the Al(2) –Al(3) bond also becomes notably weaker. This allows Al(2) atoms to supply fewer electrons to delocalized metallic Al–Al bonding and more to the localized Al(2) –B bonds, which now become more covalent in character. These observations are confirmed by features of the LDOS. There are notable changes in the Al(3) and Al(4) LDOS as shown in Fig. 5 (part II): The occupation of the Al *s* electronic states between −8 and −12 eV increases significantly compared with the GB case, indicating the increased hybridization with the B *s* states, which also show an increased occupation in this energy region. However, the most prominent changes are for the Al(2) atom, for which the LDOS now shows obvious signs of a covalent bonding: formation of two well-defined, localized *s* electronic bands and a dramatic reduction of the DOS at the Fermi level with the formation of a deep pseudogap there. The Al(2) *p* states now also become localized, with the center at −3 eV, and are hybridized with the B *p* states, and a well-defined pseudogap is formed at the E_F.

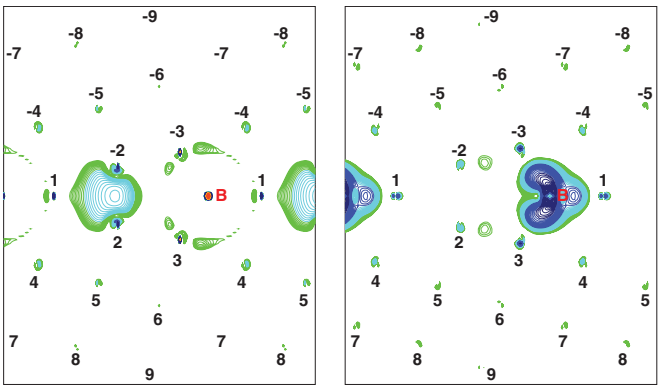

FIG. 7. (Color online) The B-induced charge density redistribution: (a) charge depletion; (b) charge accumulation. Only part of the GB with non-negligible charge difference is shown. Positions of atoms are marked with their site numbers. Contours start at ± 0.0015 $e/(\text{a.u.})^3$ (green), ± 0.0035 $e/(\text{a.u.})^3$ (blue-green), ± 0.0084 $e/(\text{a.u.})^3$ (blue), and ± 0.020 $e/(\text{a.u.})^3$ (dark blue), and increase successively by a factor of $2^{1/8}$.

To further analyze the effect that B segregation causes on the bonding character of the Al GB, the impurity-induced charge density redistribution was calculated (Fig. 7) by subtracting from the valence charge density of the Al GB with B the valence charge density of the GB system in which B is removed but the atomic coordinates of Al atoms are kept unchanged, and the valence charge density of the same GB system in which Al atoms are removed. As seen from Fig. 7(a), B segregation results in a slight charge depletion between the A(2) and Al(−2) atoms, which weakens the bonding between the GB grains. This reduction correlates with a small increase of the Al(2)–Al(−2) bond length to 4.871 a.u., compared to 4.847 a.u. in the clean GB. However, the decrease in the bonding charge is rather small (the maximum charge depletion is 0.008 $e/(\text{a.u.})^3$), which is more than compensated by the charge accumulation along the newly created B–Al(3) and B–Al(−3) bonds (Fig. 7(b)). The notably directional bonding charge distribution of B–Al bonds is characteristic for a covalent type of bonding, which confirms our analysis based on the LDOS. The asymmetry of the bonding charge distribution along the B–Al bond reflects the difference in electronegativities between B and Al (B: 2.04 and Al: 1.61), although this difference is not sufficient to change the bonding character from covalent to ionic. The maximum induced bonding charge along B–Al bonds is 0.043 $e/(\text{a.u.})^3$, which is more than five times higher than the reduction of the bonding charge for Al(2)–Al(−2) and is as high as the valence charge maximum for the Al(2)–Al(−2) bond in clean Al GB. These data attest that the main effect of segregated B on the Al GB cohesion is in creating additional bonding bridges across the two grains that are as strong as the existing Al–Al intergranular bonds and thus significantly increase GB adhesion and its resistance to breaking.

The electronic mechanism of the cohesion-enhancing effect of B discussed here is applicable not only to the Σ5(012)[100] Al GB, but to GBs with other orientations in Al alloys as well. All tilt GBs contain expansion regions near the GB

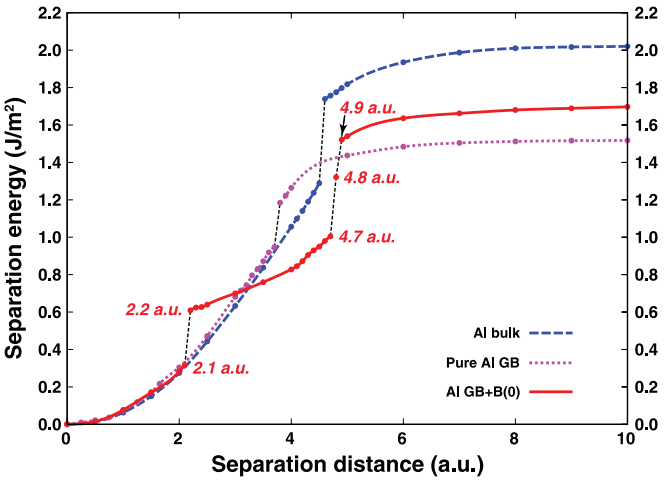

FIG. 8. (Color online) Calculated relaxed separation energies for the (012) plane of pure bulk Al, pure Al Σ5(012)[100]GB, and Al GB with a B atom at site 0, plotted as a function of separation distance

plane, which would act as preferred sites for B segregation. The segregated B atoms will strengthen the GB by creating additional B–Al bonds across the interface between grains.

VII. THEORETICAL TENSILE STRESS CALCULATIONS

To gain insight into the processes occurring during GB breaking at the atomic and electronic level, *ab initio* tensile test calculations were performed. The GB unit cell was elongated in small increments in the direction normal to the GB plane; this models the uniaxial tensile strain applied to the GB. For each elongation distance, a separation of a thickness equivalent to the unit cell elongation was initially inserted between the two grains. This separation follows fracture path II. At each elongation distance, atomic relaxations were performed, and total energies were calculated. The lateral contraction of the unit cell during the elongation (Poisson effect) was not taken into account. For more details of the *ab initio* tensile test procedure, see Ref. 12.

Figure 8 shows the calculated separation energies of the Al GB with B in site 0 as a function of separation distance, which is equal to the applied strain. The energy-separation curves for the (012) plane of bulk Al and for the pure Al Σ5(012)[100] GB are also shown for comparison; these were taken from our previous work.[12] The main quantitative characteristic of the tensile test process is fracture energy, which is defined as the limit of separation energy at infinite separation; fracture energy is a measure of the strength of the system and its resistance to crack initiation. From Fig. 8, one can see that at 10 a.u. elongation, the separation energy almost reaches saturation and is very close to extrapolated values listed in Table I. The strength of the pure Al Σ5(012)[100] GB is lower than that of Al bulk by 0.51 J/m^2, or 25%. B segregation causes a notable increase of the GB fracture energy, by 0.18 J/m^2. This result agrees with the assessment made previously based on the calculated embrittling potency: B is a cohesion enhancer for Al GB.

The separation curve for B-segregated Al GB has unique features, the analysis of which can shed additional light on the physical origins of the cohesion-enhancing effect of B.

TABLE II. Parameters of fracture energetics from theoretical tensile test calculations.

System	Fracture energy (J/m^2)	Pre-break energy (J/m^2)	Instability distance (a.u.)
Al bulk (012) plane	2.03	1.30	4.5
Al Σ5(012)[100] GB	1.52	0.95	3.7
Al GB + B (0)	1.70	1.01	4.8

As seen in Fig. 8, the separation process for bulk Al and Al GB has two distinctive parts. At small elongation distances, the system stretches elastically, and the dependence of the separation energy on elongation has a character close to parabolic. At a certain separation distance, the system reaches critical stress and cannot elongate anymore, and bond breaking occurs—usually, in an abrupt, "avalanche" manner, when the separation energy increases sharply. These avalanche breakups are marked by dashed lines in Fig. 8, and the energy points at which they occur are important characteristics of the system. Listed as prebreak energies in Table II, these energies represent the amount of energy the system can absorb before breaking up, and they also are important indicators of the system strength. The bulk Al has the highest pre-break energy of 1.30 J/m^2, or about 65% of its fracture energy, and the pre-break energy of Al GB is reduced by 27%, which is close to the relative reduction of the fracture energy. Another quantitative characteristic of the avalanche breakup process, the "instability distance," marks the expansion distance at which a breakup of the system occurs. A shorter instability distance for the Al GB compared with the bulk Al (Table II) gives an additional indication that the GB weakens the system. In the second part of the separation curves, all bonds between GB grains are broken, and the separation energy increases slowly until saturation as the remaining long-ranged interactions between the two fractured surfaces dissipate.

Unlike the pure Al bulk and the clean Al GB, the calculated relaxed separation energies of the Al GB with segregated B has three parts, with two avalanche breakups indicated by energy big jumps at small separation distance change. Similar to the cases of pure Al bulk and pure Al, the first part consists of elastic elongation of the system, with all interatomic bonds remaining intact. The first jump in separation energy occurs between 2.1 and 2.2 a.u. of separation. To reveal the changes that occur during separation at the atomic and electronic level, we will take a close look at the evolution of bonding charge densities, which are shown in Fig. 9. Between 2.1 and 2.2 a.u. of separation, two processes occur within the GB core: breaking of bonds between Al(1) and Al(4), and between B and Al(−3). Note that in the clean Al GB, the Al(1)–Al(4) bond also breaks first; however, this does not result in the avalanche increase of separation energy (see Ref. 12). Therefore, we can conclude that the first jump in the separation energy is mostly caused by breaking of the B–Al(−3) bonds. These bonds are shorter, more covalent, and therefore more rigid than the Al–Al bonds; they do not resist stretching as well as Al–Al bonds, and they break at smaller elongations. Still, after those first breakups, the GB remains connected, held together by the Al(1)–Al(2), Al(2)–Al(−2), and B–Al(1) bonds.

In the second part of the separation process, between 2.2 and 4.7 a.u. of elongation, the separation energy increases at a slower pace. During this part, the Al(2)–Al(3) and Al(2)–Al(5) bonds break, but this is compensated by the formation of a new bond between B and Al(4), which offsets the effect of breaking of two Al–Al bonds. The next critical transformation occurs between 4.7 a.u. and 4.8 a.u. of separation, where the last of intergranular B–Al(1) bonds breaks, together with the Al(1)–Al(2) and Al(2)–Al(3) bonds, causing an avalanche increase in the separation energy. Interestingly, the GB grains still remain connected via Al(2)–Al(–2) bonds, but these cannot hold the GB together for much longer, and they also break at a slight increase of strain, between 4.8 and 4.9 a.u. of elongation, producing another jump in the separation energy.

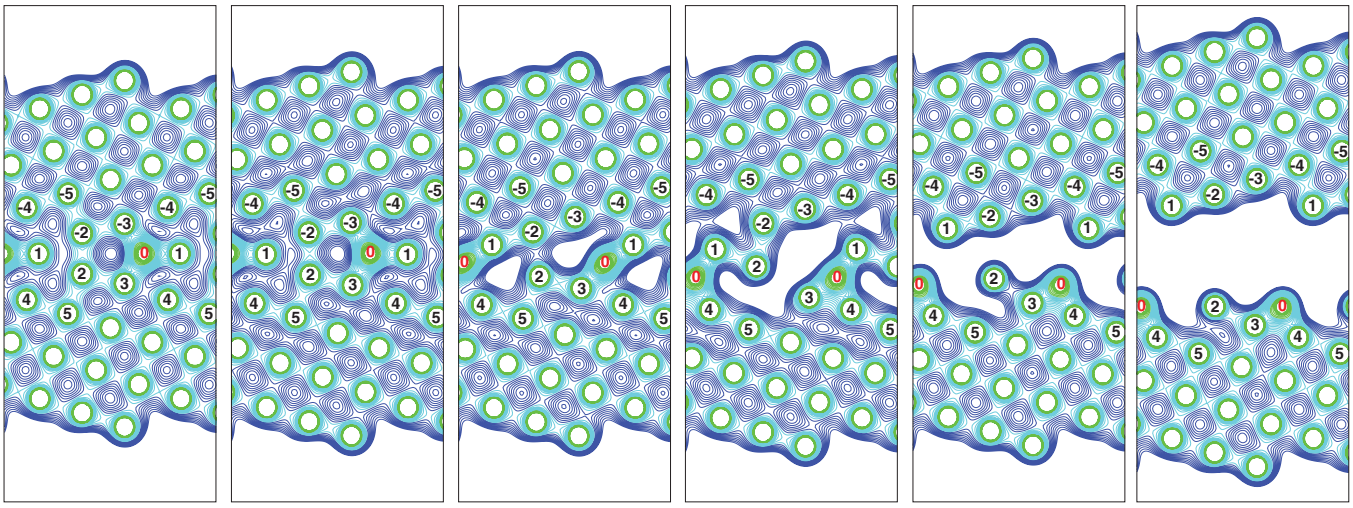

(a) *d*=0.0 a.u. (b) *d*=2.1 a.u. (c) *d*=2.2 a.u. (d) *d*=4.7 a.u. (e) *d*=4.9 a.u. (f) *d*=10.0 a.u.

FIG. 9. (Color online) Calculated charge density of Al GB with a B atom in site 1 during *ab initio* tensile test with increasing separation distance *d*. Contours start from 0.01 $e/(\text{a.u.})^3$ and increase successively by a factor of $2^{1/8}$.

The Al(2) atom moves down toward the lower grain, where it reconnects with the Al(3) atom; this reduces the energy release during the jump to 0.2 J/m^2, compared to a 0.25 J/m^2 increase in the separation energy in the case of the clean GB. Finally, at separations above 4.9 a.u., the GB is already broken, and the separation energy increases slowly until saturation as the remaining long-ranged interaction forces between the two fractured surfaces vanish.

The cleavage of an Al GB with segregated B is a complex process that involves breaking and re-creation of several interatomic bonds. Interstitial B creates new B–Al bonds that did not exist in a clean GB, and breaking them requires additional steps in the cleavage process. This staged breakup of the B-segregated Al GB allows it to sustain larger elongation, which results in a larger instability distance of 4.8 a.u., which is even larger than for pure bulk Al (see Table I). The prebreak strength of the Al GB also increases upon B segregation, thus again confirming an enhancement of the Al GB strength by B.

It should be noted that the fracture energy, which indicates the energy needed to break the structure, is a key measure of the strength of the system and its resistance to crack initiation. Thermodynamically, the work of adhesion is path independent and is a more definitive quantity than the other path-dependent quantities—the instability distance and the prebreak strength—which provides additional qualitative confirmation of the conclusions on the role of B in the Al GB based on the fracture energy and cohesion potency.

VIII. DISCUSSION

It has been long known that B improves the grain boundary strength of iron at low temperatures[16] and increases the creep resistance and ductility of steels and nickel alloys at high temperatures.[17] These effects were attributed to B segregation at GBs, which has been observed experimentally.[18,19] Boron doping improves the strength and ductility of many other structural metals and alloys, including W,[20] Ni aluminides (NiAl,[21] Ni_3Al[22]), and Ir-[23] and Pt-based alloys, [24,25] where it suppresses grain boundary fracture and changes the fracture mode to transgranular. Previous theoretical investigations have shown that B is a GB cohesion enhancer in many transition metals, including Fe,[3] Ni,[4,5] Cr,[26] Cu,[7] Nb and Mo,[6] and W.[27] The present work shows that B is also a GB cohesion enhancer in Al. From these experimental and theoretical data, B appears to be a universal GB strengthener in metals. From the analysis of the results of the present work, we can propose a mechanism for the adhesion-enhancing effect of B that is applicable not only to Al, but to other metals as well.

Traditionally, the cohesion or embrittling potency of segregated elements in GBs is attributed either to a "size effect" mechanism, where the segregate disrupts the GB bonding due to its size mismatch, or to the electronic or charge transfer mechanism, where the impurities either add or withdraw some electronic charge from neighboring host atoms, thus enhancing or reducing their cohesion across the boundary. Interestingly, these two mechanisms are often considered as opposing. In some cases, the opposite views were put forward to explain the same effect; for example, the bismuth-induced embrittlement of copper was attributed to a charge transfer mechanism by Duscher *et al.*[28] but was argued to be a purely size effect by Schweinfest *et al.*[29] In the case of B, we find that these two mechanisms work together. The size effect of an impurity is associated with the introduction of additional structural (or "mechanical," as they are often called) distortions to the GB and surrounding lattice. Boron is a small atom, the atomic size of which is almost optimal to occupy the GB hollow site that is present in all tilt GBs. As a result, B segregated to the GB causes minimal structural distortion of the GB. For example, for B in the Al GB, the structural expansion of the GB is equal to 0. In other metals and their alloys and compounds, the structural contribution can be negative or positive, but it should also be small in general. The main positive effect of B is due to the electronic mechanism. Previously, Messmer and Briant[30] proposed an electronic model to explain the effects of alloying elements on GB cohesion in metals. According to their model, the embrittling elements draw charge from the neighboring metal atoms onto themselves, thus removing charge from the metal-metal bonds that bond the GB together and weakening them; cohesive enhancers do not draw charge off the metal atoms and thus do not weaken the metal-metal bond network. This model emphasizes the charge transfer mechanism, but it would fail to predict the strengthening effect of B in Al. Indeed, according to Fig. 7, B does draw some charge from the metal-metal bonds that hold the GB together, and it weakens them. However, the more important effect of B is in creating new bonds across the GB, which more than compensate for the reduction of the metal-metal bonds. The universal cohesion-enhancing properties of B in metallic GBs result from features of its electronic structure. The atomic $2s^2 2p^1$ ground state electronic configuration of B is promoted to the $2s^1 2p^2$ configuration in the solid state, which makes both *s*- and *p*-electron shells half-filled. As a result, it is more energetically preferable for the *s* and *p* states to either become delocalized to form metallic bonding, or to become shared to participate in covalent bonding, rather than to draw electrons from neighbor atoms to fill the shells and form polar (ionic) bonds. Moreover, the bandwidth and the energy positions of the B bands are similar to those of Al and transition metals, and the difference in electronegativity for most transition metals is smaller than that between B and Al. This creates the conditions that promote hybridization between electronic states of B and metals and the formation of covalent bonding. As a result, B segregated in metallic GBs creates additional nonpolar, covalent bonding between GB grains, which holds them together and provides additional GB strengthening.

IX. CONCLUSIONS

An *ab initio* investigation was carried out to reveal the mechanism of the effect of B in the Al GB at the electronic level by means of the FLAPW method with GGA. It was shown that B exhibits a strong affinity to segregate at the Al GB hollow site from Al bulk. The influence of B on the Al GB strength was investigated both within the framework of the Rice-Wang thermodynamic model and within the *ab initio* tensile test method. Through precise calculations, both methods confirm that B is a strong intergranular cohesion

enhancer with a potency of −0.19 eV/atom. An analysis of the results in terms of relaxed atomic and electronic structures and bonding character shows that the B–Al bonding has mixed metallic-covalent character. The strengthening effect of segregated B is a result of the creation of B–Al bonds across the GB, which are as strong as existing Al–Al transgranular bonds. The B segregation leads to the strengthening of Al GB and to the increase of its work of separation. As a result, Al alloyed with small additions of B will have enhanced resistance to crack nucleation. This work provides a fundamental quantitative prediction and physical understanding of B-induced cohesion enhancement in Al alloys on the electronic level.

ACKNOWLEDGMENTS

This work was supported by the AFOSR under Grant No. FA 9550-07-1-0174 and the Ford-Boeing Nanotechnology Alliance at Northwestern University. Computer time was provided by Department of Defense Supercomputing Resource Centers AFRL, ERDC, MHPCC, and NAVY under Grant No. AFOSR15573FR1.

*shengjun-zhang@northwestern.edu

[1] J. R. Davis, *ASM Specialty Handbook: Aluminum and Aluminum Alloys* (ASM International, Materials Park (OH), 1993).
[2] M. P. Seah, Surf. Sci. **53**, 168 (1975).
[3] R. Q. Wu, A. J. Freeman, and G. B. Olson, Science **265**, 376 (1994).
[4] W. T. Geng, A. J. Freeman, R. Wu, C. B. Geller, and J. E. Raynolds, Phys. Rev. B **60**, 7149 (1999).
[5] M. Yamaguchi, M. Shiga, and H. Kaburaki, J. Phys. Condens. Matter **16**, 3933 (2004).
[6] R. Janisch and C. Elsässer, Phys. Rev. B **67**, 224101 (2003).
[7] A. Y. Lozovoi and A. T. Paxton, Phys. Rev. B **77**, 165413 (2008).
[8] J. R. Rice and J. S. Wang, Mater. Sci. Eng. A **107**, 23 (1989).
[9] E. Wimmer, H. Krakauer, M. Weinert, and A. J. Freeman, Phys. Rev. B **24**, 864 (1981).
[10] G. C. Hasson and C. Goux, Scri. Metall. **5**, 889 (1971).
[11] S. Zhang, O. Y. Kontsevoi, A. J. Freeman, and G. B. Olson, Acta Mater. **59**, 6155 (2011).
[12] S. Zhang, O. Y. Kontsevoi, A. J. Freeman, and G. B. Olson, Phys. Rev. B **82**, 224107 (2010).
[13] J. P. Perdew, K. Burke, and M. Ernzerhof, Phys. Rev. Lett. **77**, 3865 (1996).
[14] B. Cordero, V. Gomez, A. E. Platero-Prats, M. Reves, J. Echeverria, E. Cremades, F. Barragan, and S. Alvarez, Dalton Trans. **2008**, 2832 (2008).
[15] A. A. Griffith, Trans. R. Soc. Lond. A **221**, 163 (1921).
[16] H. Taga and A. Yoshikawa, Proc. ICSTIS, Suppl. Trans. ISIJ **11**, 1256 (1971).
[17] T. M. Williams, D. R. Harries, and J. Furnival, J. Iron Steel Inst. Lond. **210**, 351 (1972).
[18] D. A. Mortimer, J. Phys. Colloq. **36**, C4-137 (1975).
[19] T. M. Williams, A. M. Stoneham, and D. R. Harries, Metal Sci. **10**, 14 (1976).
[20] K. B. Povarova, Y. O. Tolstobrov, A. P. Popov, and K. I. Konovalov, Russian Metall. (Metally) **1990**, 74 (1990).
[21] E. P. George and C. T. Liu, J. Mater. Res. **5**, 754 (1990).
[22] C. T. Liu, C. L. White, and J. A. Horton, Acta Metall. **33**, 213 (1985).
[23] Y. F. Gu, Y. Yamabe-Mitarai, S. Nakazawa, and H. Harada, Mater. Sci. Eng. A **329–331**, 262 (2002).
[24] C. White, J. Keiser, and D. Braski, Metall. Mater. Trans. A **12**, 1485 (1981).
[25] J. Preußner, E. Fleischmann, R. Völkl, and U. Glatzel, Int. J. Mat. Res. **101**, 577 (2010).
[26] O. Y. Kontsevoi and A. J. Freeman (unpublished).
[27] G. L. Krasko, Int. J. Refr. Metals Hard Mat. **12**, 251 (1993-1994).
[28] G. Duscher, M. F. Chisholm, U. Alber, and M. Rühle, Nat. Mater. **3**, 627 (2004).
[29] R. Schweinfest, A. T. Paxton, and M. W. Finnis, Nature **432**, 1008 (2004).
[30] R. P. Messmer and C. L. Briant, Acta Metall. **30**, 457 (1982).